Proceedings World Geothermal Congress 2020+1
Reykjavik, Iceland, April - October 2021

Glacial Influence on Hydrogeology and Geothermal Potential in the North Alpine Foreland Basin – A Fossil Temperature Imprint in the Upper Jurassic Carbonate Aquifer?

Tom V. Schintgen[1] and Inga S. Moeck[1,2]

[1]Leibniz Institute for Applied Geophysics (LIAG), Stilleweg 2 30655 Hannover, Germany

[2]Georg-August-Universität , Goldschmidtstraße 3 37077 Göttingen, Germany

tom.schintgen@leibniz-liag.de

Keywords: Würm Glaciation, North Alpine Foreland Basin, Molasse Basin, Upper Jurassic, Malm, carbonate aquifer, coupled heat and fluid flow, gravity-driven groundwater flow, Play Type

ABSTRACT

The geology, structures and stratigraphy of the North Alpine Foreland Basin, more specifically of the Molasse Basin in southern Germany and Austria, have been studied for decades and used as a basis first for oil & gas exploration and exploitation, and more recently for geothermal energy applications. In the Molasse Basin in particular, geothermal exploration risk and the operation of the numerous existing as well as planned geothermal installations critically depends on an accurate prognosis of both permeability and temperature within the Upper Jurassic (Malm) carbonate aquifer. Many boreholes tap the Malm aquifer mainly for district heating, balneological use, but also for electricity production. We study the coupled, thermal-hydraulic processes in this foreland basin play under paleo-climatic conditions spanning the last glaciation (Würm) by investigating specifically the origin of the prominent cold thermal anomaly located to the (north) -east of Munich. The existence of cold thermal anomalies represents a high risk for geothermal energy exploration. We are able to reproduce the thermal anomaly by varying the carbonate permeability at the Danube between high values of 10^{-10} m^2 for karstified zones and low values of 10^{-13} m^2 for carbonate facies less prone to karstification. Gravity-driven groundwater flow related to high carbonate permeability is shown to significantly affect the heat flow and thus the thermal field in the molasse sediments and the Malm aquifer. The findings are an important contribution to the characterization of the foreland basin play type which aims at comparing similar geological settings worldwide.

1. INTRODUCTION

The classical approach in geothermal exploration consists in cataloguing geothermal resources according to temperature or depth mainly for technical and economic reasons. The recent geothermal Play-Type concept ((Moeck 2014; Moeck and Beardsmore 2014; Moeck et al. 2015) aims at classifying geothermal resources according to geological criteria and heat transport mechanisms to assess reservoir quality. Internationally applicable criteria allow worldwide comparisons between resources of similar geological settings and structures (play type). The method applied in this study is numerical thermal-hydraulic modelling. The selection of reference plays like the Molasse Basin, the German part of the North Alpine Foreland Basin, ensures that the assessment of geothermal resources is based on geological criteria.

Among the German geothermal provinces, the Molasse Basin in southern Germany has been studied for decades for its geology, structures and stratigraphy (Freudenberger and Schwerd 1996), for oil and gas (Bachmann et al. 1982; Bachmann and Mueller 1992; Bachmann et al. 1987; Brink et al. 1992; Reischenbacher and Sachsenhofer 2011; Sachsenhofer et al. 2006), and more recently for geothermal energy (Birner et al. 2012; Böhm 2012; GeoMol Team 2015; Jodocy and Stober 2009). Many boreholes tap the Upper Jurassic (Malm) carbonate aquifer mainly for district heating and balneological use, but also for electricity generation. The Malm carbonate aquifer is considered to be the largest thermal water resource not only in Germany but also in Central Europe (Goldscheider et al. 2010). Indeed, carbonate aquifers frequently present a high secondary porosity and permeability due to karstification.

The Molasse basin has been studied hydrogeologically (Andres and Frisch 1981; Frisch and Huber 2000), and recently by coupled heat and fluid flow (Przybycin et al. 2017). However, the geostatistical assessment of the 3D thermal structure based on temperature measurements in boreholes (i.e. the GeotIS composite model) to date represents the most reliable prognosis of subsurface temperature in the Molasse Basin (Agemar and Tribbensee 2018). The prominent cold temperature anomaly to the east and northeast of Munich presents a particular high geothermal exploration risk and therefore was the subject of recent studies.

Similar to studies in the Alberta, North German and Paris basins, we use the COMSOL Multiphysics software to perform thermal-hydraulic modelling of the glacial influence on the present-day thermal and flow regime in the Molasse Basin. The result is compared with the geostatistically evaluated 3D thermal field. By contrast to several existing studies, we focus on the assessment of the main fluid and heat transport processes for a better understanding of thermal anomalies induced by gravity-driven groundwater flow and paleo-climatic conditions. Cross-formational gravity-flow of groundwater is long known to act on geological timescales and it is obviously very important to quantify its effect in the foreland basin play type. The driving forces of regional gravity-driven groundwater flow systems are largely controlled by the configuration of the water table. Under most conditions, the water table corresponds to the topography and its configuration determines the hydraulic head distribution (Seguinot et al. 2018; Toth 2009).

1.1 Geological evolution

The Molasse Basin in southern Germany and Upper Austria is part of the North Alpine Foreland Basin (NAFB). In Germany, it is up to130 km wide perpendicular to strike and 400 km long parallel to the Alps (Figure 1). The depth of the Upper Jurassic carbonates reaches op to 5000 m close to the Alpine front (Bachmann and Mueller 1992; Reinecker et al. 2010).

In southern Germany, marine transgression at the beginning of the Jurassic led to progressive flooding of the Vindelician High and thus submergence of the Variscan basement. In the Upper Jurassic (Malm), a carbonate platform formed under varying conditions on an epicontinental shelf (Birner et al. 2012; Freudenberger and Schwerd 1996; Frisch and Huber 2000). On the deeper shelf, in the southern and southwestern part of the Molasse Basin, rather dark carbonates rich in clay and organic material accumulated pertaining to the so-called Helvetic facies, being characterized by a generally very low hydraulic conductivity. In a northerly direction and towards the northwest, on the higher shelf, and in between reef complexes, carbonate sedimentation led to the formation of the stratified facies called 'Schichtfazies' with interbedded marls. The latter is also characterized by a relatively low hydraulic conductivity. Towards the east and northeast, mainly in the Bavarian and Austrian part of the Molasse Basin, carbonate accumulation formed the reef facies on top of submarine barriers in a higher energy environment (Frisch and Huber 2000; Meyer and Schmidt-Kaler 1990). These massive reef carbonates have the highest hydraulic conductivities and are prone to karstification (Birner 2013; Birner et al. 2012). After the maximum extension of sponge reefs in the Malm Delta, the shallowing sea caused the disintegration of the reef platform into smaller units (Meyer and Schmidt-Kaler 1990). Only in the Late Jurassic, the regression caused the sea to retreat into the deepest parts of the basin, the Wasserburg Trough (Figure 1).

The southeasterly emersion of the up to 600-m-thick Upper Jurassic carbonates initiated an extensive karstification which affected the upper 150 to 200 m of the massive carbonates of the reef facies in the central and eastern parts of the Molasse Basin (Frisch and Huber 2000). The duration of karstification in Cretaceous times is about 45 Ma. By contrast to karst systems in the west, the rapid burial by Cretaceous sediments in the east appears to have caused a better preservation of these karst systems which are presently characterized by extraordinary high permeabilities (Frisch and Huber 2000).

The pre-Tertiary sediments and thus the foreland basin began to subside during the Late Eocene (Schmid et al. 2004), followed by the deposition of Lower Oligocene flysch units and of orogen-derived continental clastics (i.e., the Molasse or molasse sediments) during the late Oligocene to late Miocene (Roeder and Bachmann 1996). The post-flysch (Oligocene - Miocene) paleogeographic evolution of the entire North Alpine Foreland Basin (NAFB) and the facies distribution in the NAFB was driven by two major types of processes, which are related to the tectonic evolution of the Alpine orogeny (Kuhlemann and Kempf 2002; Schmid et al. 2004): (1) a direct influence by tectonic processes at the thrust front, and (2) an indirect impact of Alpine uplift and tectonics, transformed by varying sediment discharge.

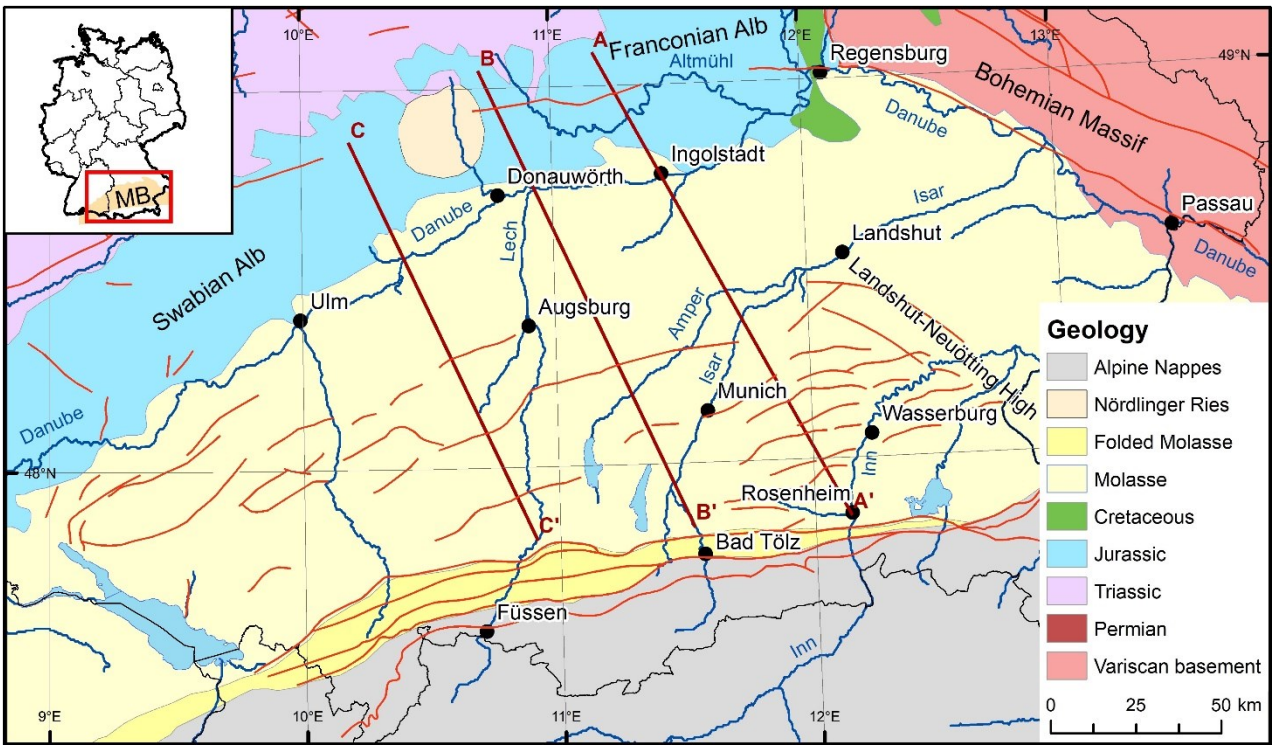

Figure 1: Regional geological map of the Molasse Basin. Inset map shows location of the map in Germany (MB = Molasse Basin). Dark red lines (AA', BB', CC') indicate representative cross sections. Red lines represent faults (in the Molasse Basin) or thrusts (in the Folded Molasse and Alpine nappes).

1.2 Present geological and structural setting

Today, the Upper Jurassic carbonates form the Swabian and Franconian Albs or Jura to the north of the Danube river (Figure 1). To the south, the carbonate platform is dipping beneath the southwards thickening Tertiary molasse sediments (Figure 1). Lying at a depth of about 2000 m below Munich, the top of the carbonates reach a depth of more than 4000 m at the Alpine front (Brink et al. 1992). The molasse sediments are composed of cyclically deposited clayey and sandy series, which are subdivided from bottom to top into Lower Marine Molasse, Lower Freshwater Molasse, Upper Marine Molasse and Upper Freshwater Molasse (GeoMol Team 2015). The basement is known from the Variscan Bohemian Massif in the east and northeast (Figure 1) where the Malm terminates against the Danube Boundary Fault and the basement is uplifted up to 1700 m (Frisch and Huber 2000). In front of the boundary fault

of the Bohemian Massif, another important basement structure, the NW–SE-oriented horst of the Landshut-Neuöttinger Hoch (LNH; Figure 1) with a throw of up to 1300 m separates the Wasserburg Trough in the west from the Lower Bavaria Trough in the east (Bachmann et al. 1987; Frisch and Huber 2000).

The Molasse Basin contains numerous faults which are related to thrusting and uplift of the Alps and the contemporaneous downbending of the European plate and formation of the Molasse Basin (Schmid et al. 2004). In the western and central parts, the W-E striking faults parallel to the basin axis and to the Alps were formed as synthetic and antithetic faults due to downbending and extension of the top of the European crust (Bachmann et al. 1982; Brink et al. 1992). In the eastern part, the WNW-striking faults are related to the uplift of the LNH and the Bohemian Massif (Bachmann et al. 1987).

1.3 Hydrogeological data and models

In the western Molasse Basin, Rühaak (2009) conclude that deviations from their 3D steady-state and conductive model are likely caused by advective heat flow especially in fault zones. Frisch and Huber (2000) present a numerical groundwater model for thermal water mass balancing and deduce flow directions within the Upper Jurassic aquifer. Birner et al. (2012) clearly shows that high hydraulic conductivities are closely linked to karstified zones in relation with the reef carbonate facies, faults and the proximity of the Danube. A remarkable fact is the sub-hydrostatic character of the Malm aquifer (Lemcke and Tunn 1956) with a water table well below terrain level towards the Alpine front and local artesian conditions close to the Danube (Andres and Frisch 1981; Frisch and Huber 2000). Aquifer recharge occurs on the one hand along the Danube river and especially to the north of it through the outcropping Upper Jurassic and on the other hand by leakage through the overlying Quaternary and Tertiary sediments (Andres and Frisch 1981; Frisch and Huber 2000). The general groundwater flow is directed from the west to the east and thus follows the gradient of the Danube (Birner 2013; Frisch and Huber 2000). By contrast to other sedimentary basins, the existence of freshwater with a mineralization below 1g/L in the Malm aquifer in large areas of the Molasse Basin (Frisch and Huber 2000; Stober et al. 2014) is a strong argument for the good hydraulical connection with the Danube.

Przybycin et al. (2017) performed 3D numerical modelling of coupled fluid and heat flow processes in the Molasse Basin. The results by Przybycin et al. (2017) show that the shallow thermal field is strongly affected by basin-wide fluid flow. They assign a strong thermal impact to the hydraulic conductivity of the Molasse sediments, but only a low thermal influence to hydraulically conductive faults in the Upper Jurassic carbonate aquifer. However, Przybycin et al. (2017) put forward that some misfit between observed and modelled subsurface temperatures results from the relatively coarse resolution, a lack of details and the need for a better knowledge of thermal and hydraulic properties.

Despite the existing numerical models, the geostatistical assessment of the 3D thermal structure based on temperature measurements in boreholes (i.e. the GeotIS composite model; Figure 2) to date represents the most reliable prognosis of subsurface temperature in the Molasse Basin (Agemar and Tribbensee 2018). Strikingly, a prominent cold temperature anomaly to the east and northeast of Munich could not yet be satisfactorily explained.

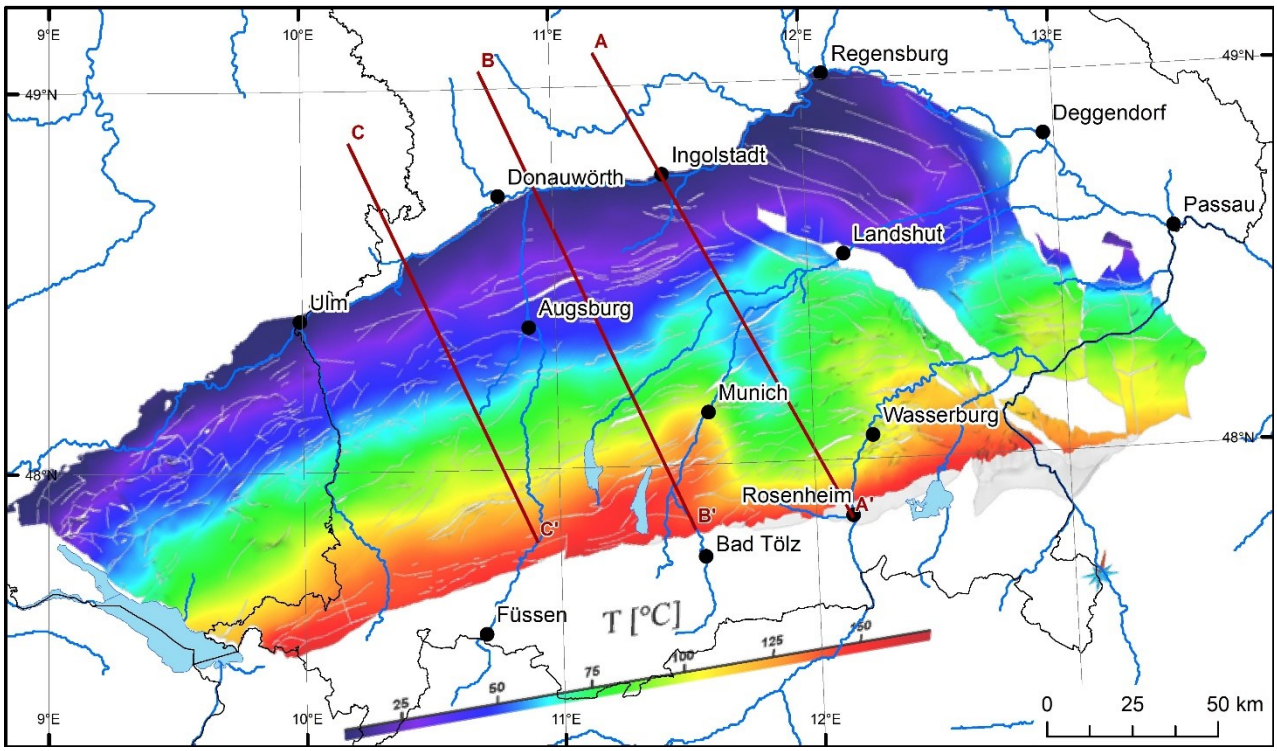

Figure 2: 3D structural model of the Top Malm (Upper Jurassic) for Baden-Württemberg, Bavaria and Upper Austria. The temperature distribution is derived from the geostatistical 3D temperature model of the LIAG (Agemar and Tribbensee 2018).

2. METHODOLOGY AND MODEL SET-UP

We use COMSOL Multiphysics to simulate coupled heat and fluid flow in the Molasse Basin. For a faster computation of the basic physical, thermal-hydraulic processes, we built a 2D section oriented perpendicular to the strike direction of the Molasse Basin and containing only the most important geological and structural elements (Figure 3). The model section represents the geometrical situation to the east and northeast of the region of Munich where a prominent cold anomaly occurs (Agemar and Tribbensee 2018). It is oriented NNW-SSE and extends 180 km from the northern margin of the Franconian Alb via Ingolstadt to Rosenheim close to the Alpine Front (Figures 1 and 2). Model depth amounts to 10 km below mean sea level. The model is set up for multiphysics coupling of the porous media and subsurface flow module using Darcy's Law and the heat transfer in porous media module. The study is time-dependent and simulates the last 130,000 years to capture the effects of the paleotemperature changes on the subsurface thermal field. The model represents three main regions (Figure 3): (1) the Franconian Alb composed of a several hundred meters-thick Upper Jurassic carbonate platform overlying a mostly Variscan basement composed of gneiss and intrusions of igneous rock (mainly granite), (2) the interfluve between the Altmühl and Danube rivers of basically similar geological configuration, and (3) the Molasse Basin itself composed of a wedge of Molasse sediments whose base reaches 5,000 m below mean sea level at the Alpine Front, underlain by a 500-m-thick layer of Upper Jurassic carbonate (Malm aquifer), the latter resting on the Variscan basement.

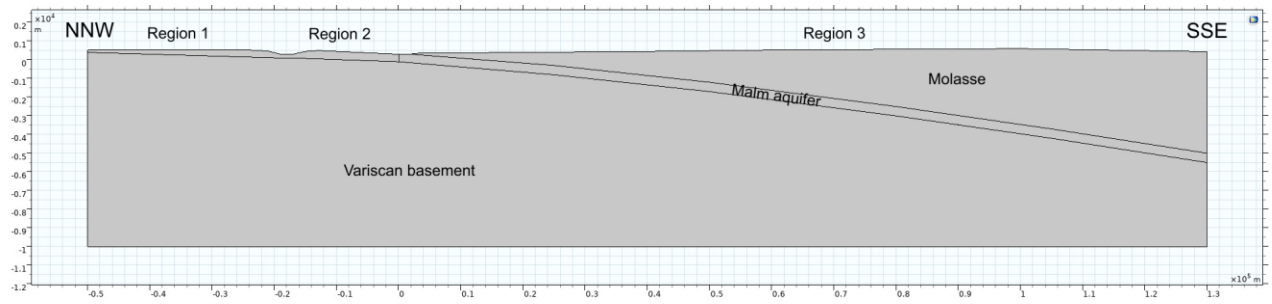

Figure 3: Simplified geometry along cross section AA' implemented in the model. It spans from the Franconian Alb in the north (left) over Ingolstadt to Rosenheim close to the Alpine Front in the south (right). For details about the regions, see text.

The paleo-temperature data are among the most important model input data (Figure 4). This climate forcing is derived using time-dependent temperature offsets from a paleo-climate proxy. For the present study, we chose the EPICA ice core record (Jouzel et al. 2007) which, in a glaciological study by Seguinot et al. (2018), yielded spatially and temporally consistent ice dynamics. Climate forcing is amended with temperature lapse-rate corrections, time-dependent temperature offsets and time-dependent paleo-precipitation reductions.

2.1 Paleo-climate forcing

2.1.1 Paleo-temperature forcing

Following (Seguinot et al. 2018), temperature offset time-series are derived from paleo-temperature proxy records from the European Project for Ice Coring in Antarctica (EPICA; Jouzel et al. (2007)). Temperature reconstructions from the EPICA record are provided and can be downloaded e.g. from the PANGAEA data repository. The time resolution of the data decreases with age from 10 years to 45 years at 130 ka. For simulation, time steps of 50 years are used. The paleo-temperature model input data were smoothed by applying a running average of 21 values and adding an additional running average of 11 values on top of the first (Figure 4).

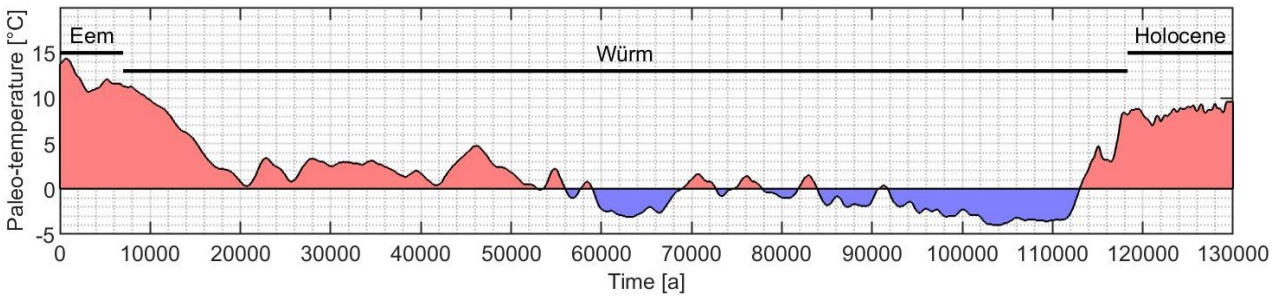

Figure 4: Paleo-temperature for a reference mean annual surface temperature of 9°C and 300 m altitude modified from the European Project for Ice Coring in Antarctica (EPICA; Jouzel et al. 2007). Linear scaling for paleo-precipitation forcing implemented following Seguinot et al. (2018). Red and blue coloring represents mean annual surface temperature above and below zero degrees C, respectively. Time axis inverted for computation.

2.1.2 Paleo-precipitation forcing

Seguinot et al. (2018) reduced precipitation with air temperature in order to simulate the potential rarefaction of atmospheric moisture in colder climates. The derived relationship results in about 60% less precipitation at the Last Glacial Maximum (LGM). Accordingly,

the linear scaling (f = 1.33) used by Seguinot et al. (2018) was also implemented in this study to calibrate the paleo-temperature forcing in the light of reduced precipitation.

2.1.3 Temperature lapse-rate correction

According to a present-day mean annual surface temperature map (e.g., Hänel and Staroste (1988)), and altitude information, reference temperatures of 9°C at 300 m and of 5°C at 1000 m were determined. The result for Munich at 520 m altitude is 7.7°C and consequently the temperature lapse rate in this part of the North Alpine Foreland corresponds to 0.571°C/100 m. In the Danube and Altmühl valley, but also in the Franconian Alb, freezing and permafrost formation is avoided for numerical stability reasons by disabling the temperature lapse rate and by restricting the minimum temperature to 4°C. These simplified temperature conditions barely influence the main findings.

2.2 Model boundary conditions

Boundary conditions are defined separately for each module.

2.2.1 Subsurface flow boundary conditions

At the vertical boundaries delimiting the model in the north and the south as well as at the bottom boundary, no-flow conditions are set. In the Altmühl and Danube valleys where groundwater is allowed to flow towards major rivers, an atmosphere/gauge boundary condition is set. In the northern part of the model corresponding to the Franconian Alb, a hydraulic head in equilibrium with the major bounding rivers is specified. In the southern part of the model corresponding to the surface of the molasse, a hydraulic head replicating the topography is applied. It should be noted that, along the chosen section, the slope towards the Alpine front reaches its maximum altitude of 600 m 30 km to the north of Rosenheim from where the altitude decreases again southwards in the direction of Rosenheim and the Inn valley. This topographic profile has important implications for groundwater and heat flow. For the specification of initial values, a hydraulic head in accordance with the Molasse surface topography is defined in order to ensure the lowest deviations.

2.2.2 Heat transfer boundary conditions

At the vertical boundaries, no-flow conditions for heat transfer are set. At the bottom, a basal heat flow ranging between 60 mW/m^2 in the south and 70 mW/m^2 in the north is defined. Additional radiogenic heat production in the Variscan basement ($1.8*10^{-6}$ W m^{-3}) and in the Molasse sediments ($1.2*10^{-6}$ W m^{-3}) cause a conductive surface heat flow density value ranging between 87 mW m^{-2} in the north and 75 mW/m^{-2} in the south. At the upper boundary, paleo-climate forcing is applied (see section 2.1). A look at the top Malm temperatures (Agemar and Tribbensee 2018) in combination with the course of rivers reveals an overlay of the Amper and Isar valleys with the coldest zone of the underlying thermal anomaly. Since permafrost may be absent below rivers and lakes, it is possible that cold groundwater is able to infiltrate in the Amper and Isar valleys even at cold surface temperatures. For the specification of initial temperature values, the thermal field is defined by a thermal gradient of 30°C/km yielding temperatures of about 309°C at 10 km depth at the model base.

2.3 Temperature- (and pressure-) dependent material properties

Since glacial and periglacial climate conditions are taken into account, the formation of permafrost is implemented by using the phase change material sub-node of the heat transfer in porous media module. The transition temperature is 273.15 K, the transition interval is 1 K and the latent heat of fusion is 333.5 kJ/kg. The required data are presented in Table 1.

Table 1: Material properties for ice and water used in the model.

Material property	Ice (< 273.15 K)	Water (> 273.15 K)
Density	918 kg/m^3	997 kg/m^3
Heat capacity at constant pressure	2052 J/(kg*K)	4179 J/(kg*K)
Thermal conductivity	2.31 W/(m*K)	0.5713 W/(m*K)

The simulation of coupled heat and fluid flow requires the following fluid properties: dynamic viscosity, density, heat capacity at constant pressure and thermal conductivity.

2.3.1 Ice (phase 1)

In the model, ice only exists over a small temperature interval, so that it is considered independent of temperature and pressure.

2.3.2 Water (phase 2)

It is assumed that water is pure, which is a valid assumption since the Malm aquifer has drinking water quality (Frisch and Huber 2000; Stober et al. 2014). Furthermore, hydrostatic fluid pressure is assumed to prevail throughout the model domain. We are aware that fluid pressure may tend to lithostatic with depth and that the content in dissolved solids certainly increases in the Variscan basement, but no data for this depth realm are available. Water density would remain almost constant with depth and dynamic viscosity increase due to dissolved solids.

By default, the properties of water are temperature-dependent in COMSOL. However, since our model extends to a depth of 10 km, we also evaluated the effect of pressure by consulting the international steam tables (Wagner and Kretzschmar 2008). Based on

previous model runs, realistic temperature and hydrostatic pressure gradients were chosen (25°C/km and 95 bar/km, respectively). Along the selected T-P-gradient, all relevant water properties show significant changes, ranging from +14% for thermal conductivity and -92.5% for dynamic viscosity. The decrease in water density (19%) is important because shallower colder water has a tendency to sink, whereas deeper warmer water tends to ascend. The buoyancy of deep hot water actually induces a hydraulic head at depth which acts against the hydraulic head related to the water table and thus topography. Both hydraulic heads are directed towards the carbonate aquifer.

2.4 Definition of geological units

The properties assigned to the geological units are given in Table 2.

2.4.1 Variscan basement

The Variscan basement is mainly made up of gneiss and granitic intrusions. Its permeability is assumed to be isotropic, but to decrease by three orders of magnitude from the top to the bottom of the model. The thermal conductivity of these metamorphic rocks is temperature-corrected with rock-specific coefficients (Schintgen et al. 2015; Seipold 2001). Due to this correction, the thermal conductivity of the basement progressively decreases with temperature to 77% of its surface value towards the bottom of the model.

2.4.2 Upper Jurassic carbonate (Malm aquifer)

The Upper Jurassic carbonate platform is made up of different facies which, however, are not differentiated in the present study. Its permeability is assumed to be anisotropic and one order of magnitude higher in horizontal direction because of the preferential development of karstic conduits along specific bedding planes. Permeability increases linearly from the south towards the Danube river. To the north of the Danube river, in the unconfined carbonate, the permeability is assumed to be isotropic and high (10^{-10} m^2). The thermal conductivity of these carbonates is temperature-corrected using the equation for sediments by Somerton (1992) (Schintgen et al. 2015). Due to this correction, the thermal conductivity of the carbonates progressively decreases with temperature to 82% of its surface value.

2.4.3 Tertiary Molasse sediments

The Tertiary Molasse sediments are composed of clay, silt, sand and gravel layers which are not differentiated in the present study. The permeability of the Molasse is assumed to be anisotropic and one order of magnitude higher in horizontal direction because the interbedded more permeable sand and gravel layers likely enhance groundwater flow horizontally. The thermal conductivity of the Molasse is temperature-corrected using the equation for sediments by Somerton (1992) (Schintgen et al. 2015). Due to this correction, the thermal conductivity of the Molasse sediments progressively decreases with temperature to 88% of its surface value.

Table 2: Properties of the geological units implemented in the model.

Geological unit	Porosity [-]	Permeabillity [m^2]		Thermal conductivity [W m^{-1} K^{-1}]	Density [kg m^{-3}]	Isobaric heat capacity [J kg^{-1} K^{-1}]
		horizontal	vertical			
Molasse	0.20	10^{-14}	10^{-15}	2.0	2000	800
Upper Jurassic carbonate (Malm)	0.10	10^{-10} – 10^{-14}	10^{-11} – 10^{-15}	2.5	2400	900
Variscan basement	0.03	10^{-17} – 10^{-20}	10^{-17} – 10^{-20}	3.5	2700	900

3. RESULTS

Permeability of the Upper Jurassic (Malm) carbonate aquifer is varied linearly from very low (anisotropic) values of 10^{-15} m^2 horizontally and 10^{-16} m^2 vertically in the southernmost part of the model to high (anisotropic) permeability values in the Danube valley. In multiple model runs, the permeability tensor is varied by four orders of magnitude from 10^{-14} m^2 horizontally and 10^{-15} m^2 vertically to 10^{-10} m^2 horizontally and 10^{-11} m^2 vertically (Figure 5). The main observation is that for low horizontal permeabilities of 10^{-14} m^2 and 10^{-13} m^2 groundwater flow is essentially limited to the molasse sediments and does not flow towards the Malm aquifer. As a consequence, cooling of the shallow subsurface is mostly restricted to the molasse and does not affect the Malm aquifer (Figure 5b). By contrast, if the horizontal carbonate permeability equals 10^{-13} m^2 and higher, groundwater flow circulation is no longer within the molasse sediments but descends into the Malm aquifer. As a consequence, subsurface cooling also extends to significantly greater depth (Figure 5a). The general flow pattern results from the downflow of cold meteoric water through the molasse, slow heating of this water and finally upflow of the heated groundwater through the carbonate aquifer to the surface in the Danube valley. The coupled fluid and heat flow thereby significantly modifies the original, homogeneous geothermal gradient (Figure 5).

A different maximum permafrost thickness is observed depending on the maximum horizontal carbonate permeability of 10^{-10} and 10^{-13} m^2, respectively (Figure 6). In general, cooling of the shallow subsurface is much more pronounced in case the carbonate permeability is 10^{-10} m^2 at the Danube (Figures 5a and 6a). When paleo-temperatures start to decrease, cold water downflow through the Molasse sediments is seen as a dark blue curtain moving down towards the Malm aquifer. About 35 ka ago (95ka in Figure 4), at the start of the coldest period of the last glaciation, permafrost develops to greater depth where cold water had previously flown down (Figure 6). Permafrost thickness reaches on average up to 700 m in the scenario with a horizontal permeability of 10^{-10} m^2 at the Danube (Figure 6a). As a comparison, permafrost thickness is only 150–200 m in case of the low permeability bound (Figure 6b). At

the end of the LGM, permafrost has largely melted 15 ka ago, but patches of permafrost remain until about 10 ka. Again, after the permafrost has melted, cold water downflow is seen as a dark blue curtain. The effect of permafrost formation and meltdown is regionalization of cold water downflow over the entire width of the Molasse Basin. Indeed, after 10 ka of simulation time, the 20, 40 and 60°C-isotherms show a maximum downward curvature between profile km 45 and 65 where groundwater mass flux is highest due to the very high carbonate permeability and the relatively low thickness of the molasse sediments in the range of 1500 to 2500 m. After 30 ka of simulation time, the maximum downward curvature of these isotherms has shifted southwards to a zone between profile km 60 and 75. After 50 ka of simulation time, the maximum downward curvature of the 20°C-isotherm is located at profile km 65. A second downward curvature begins to develop underneath the highest hydraulic head at profile km 100. After 70 ka of simulation time and the first phase of permafrost formation, the 20, 40 and 60°C-isotherms have become almost horizontal between profile km 60 and 100, i.e. parallel to the base of permafrost (Figure 6a). The latter zone extends even further between profile km 50 and 110 after the LGM 20 ka ago (i.e. 110 ka of simulation time; Figure 6). In the southernmost part of the model where the surface falls off towards the Inn valley and Rosenheim, groundwater flow descends from the highest hydraulic head at 600 m altitude and ascends in the vicinity of the Inn valley (Figures 5 and 6). This groundwater thus forms a separate convection cell which is decoupled from the flow heading towards the Malm aquifer and to the north. Thereby the upflow of groundwater and heat causes the isotherms to rise so that temperatures at the same depth increase by about 40°C.

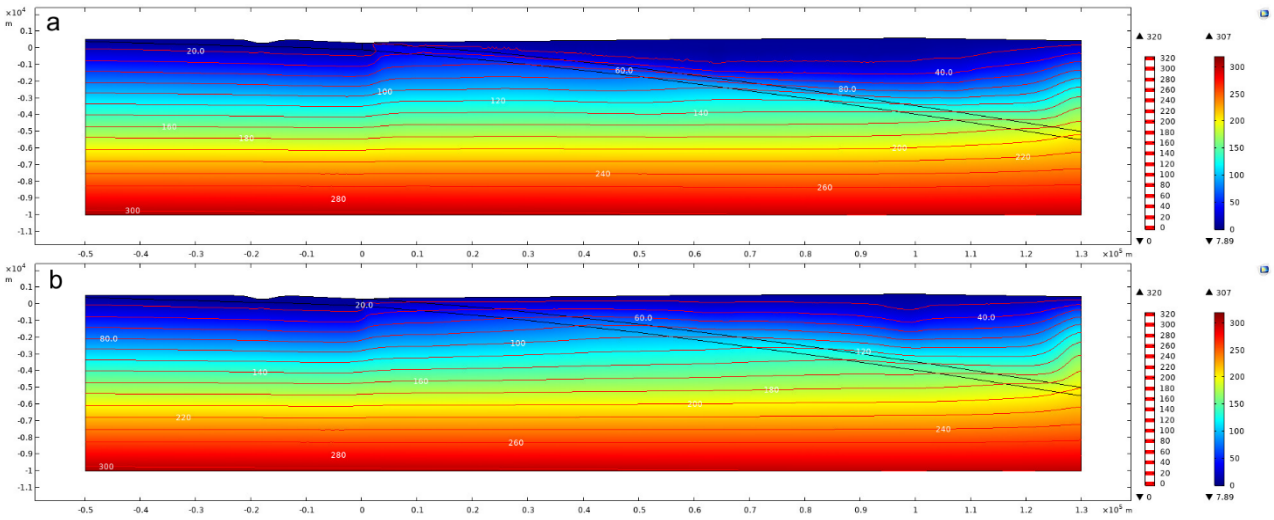

Figure 5: Temperature plot (in °C) at 130 ka representing the present-day: for a maximum permeability of 10^{-10} m^2 (top) and 10^{-13} m^2 (bottom) at the Danube, respectively. The vertical exaggeration factor equals 3.

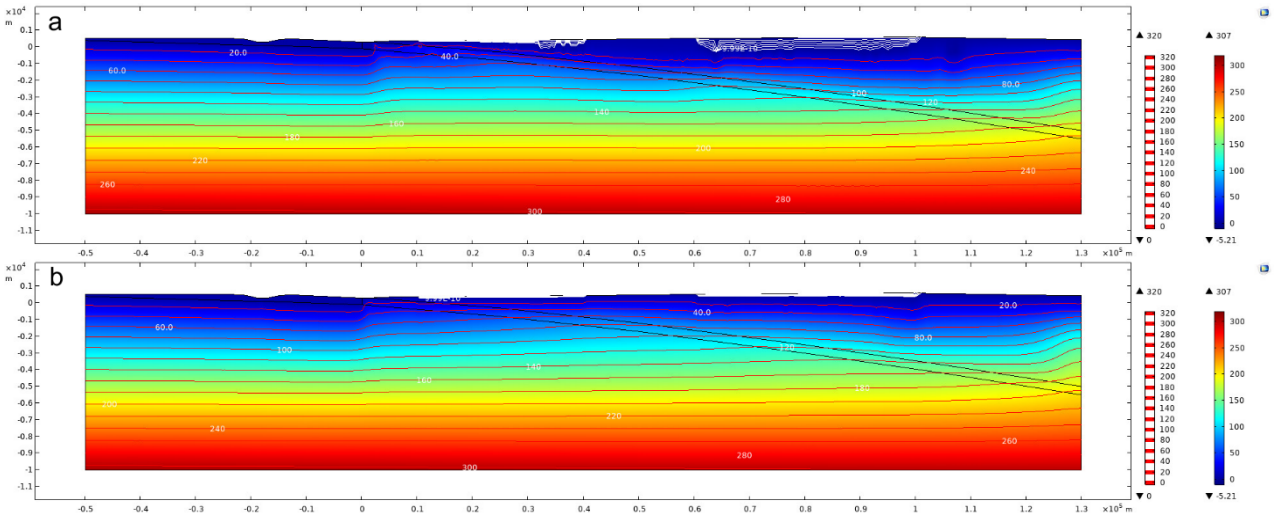

Figure 6: Temperature plot (in °C) at 110 ka representing the end of the Late Glacial Maximum: for a maximum permeability of 10^{-10} m^2 (top) and 10^{-13} m^2 (bottom) at the Danube, respectively. The vertical exaggeration factor equals 3. Note the very different permafrost thickness.

After several model runs with parameter changes it is possible to join data sets in order to combine two solutions and to show the difference between the solutions over time. By simulating for instance the hydraulic effect of the Inn Glacier on subsurface flow in the Molasse Basin, the results clearly show that the hydraulic head in the southernmost part of the model periodically increases when

the Inn Glacier advances onto the foreland, but that the thermal field is barely influenced by a supposedly higher quantity of cold water infiltrating into the basin.

More illustrative than the absolute thermal field shown in Figures 5 and 6 is the temperature difference over time between the scenarios with high and low carbonate permeability at the Danube shown in Figure 7. A cold thermal anomaly has developed in the northern part of the molasses wedge after 20 ka and gets colder with time. Later, e.g. at 110 and 130 ka it extends through the Malm aquifer and beyond into the Variscan basement (Figure 6a and c). In addition, the cold thermal anomaly observed at the southern boundary of the latter sections is related to the Inn Glacier that advances periodically onto the Molasse Basin and imposes a high hydraulic head and so pushes cold meltwater into the subsurface. The red colors in Figure 7 represent the upflow of warmer water through the Malm aquifer towards the Danube in case the carbonate permeability is high. This shows that cooling of the Molasse in the downflow zone results in heat transfer towards the Danube in the upflow zone.

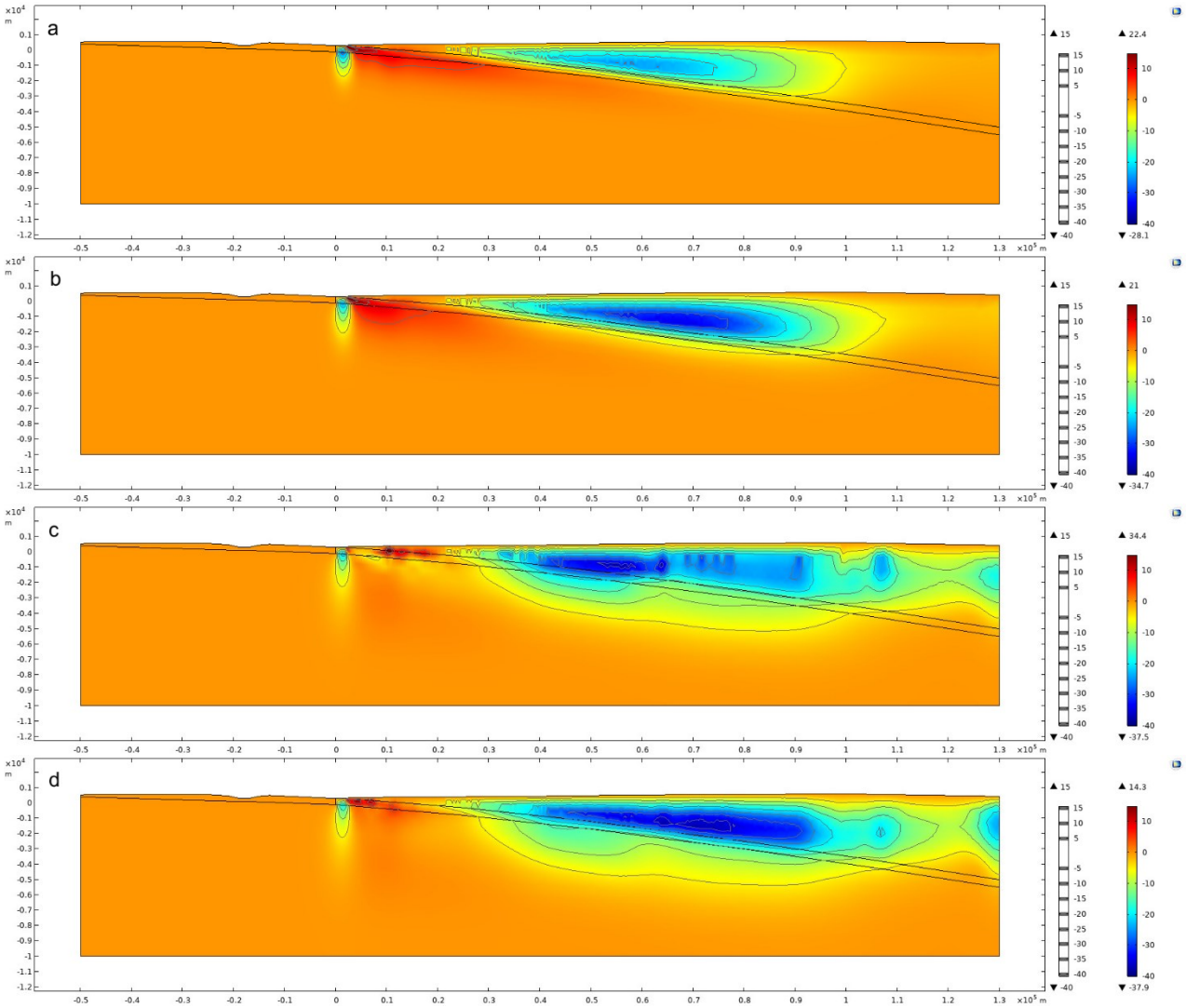

Figure 7: Temperature difference plots (in °C) at (a) 20, (b) 40, (c) 110 and (b) 130 ka (the latter representing the present day) between both scenarios of maximum permeability of 10^{-10} and 10^{-13} m^2 at the Danube, respectively. The vertical exaggeration factor equals 3.

In order to validate the effect of periglacial climate conditions and thus paleo-temperature forcing on coupled, gravity-driven groundwater and heat flow, we also simulated both permeability scenarios with a constant reference temperature of 9°C at 300 m altitude as a surface boundary condition. The resulting thermal fields after 130 ka look similar to the sections in Figure 5a and b, respectively. The calculated temperature difference shown in Figure 8 reveals a cold thermal anomaly centered on the Molasse Basin. Temperatures in the Molasse at about 2000 m depth are up to 50°C colder in case of carbonate permeability of 10^{-10} m^2 at the Danube. For high carbonate permeabilities, water temperature is up to 17°C warmer in the vicinity of the Danube (Figure 8). Again, for a clear visualization of the differences between Figures 7 and 8, Figure 9 shows the temperature difference for each permeability scenario with paleo-climate considered and the corresponding model with constant reference surface temperature. A very cold thermal anomaly with temperatures more than 100°C colder is observed in both temperature sections in the southernmost part of the models. In both temperature sections, a few degrees C colder temperatures are observed beneath the exposed carbonate in the Franconian Alb. Equally, thermal anomalies colder than -2 to -4°C are observed relatively close to the surface in both sections. However, the major difference between both sections in Figure 9 is a large thermal anomaly up to about 16 °C warmer centered on the Molasse Basin and

the Malm aquifer in case of high carbonate permeability (Figure 9a), and a smaller thermal anomaly up to 12.5°C warmer in the southern part of the model in case of low carbonate permeability (Figure 9b).

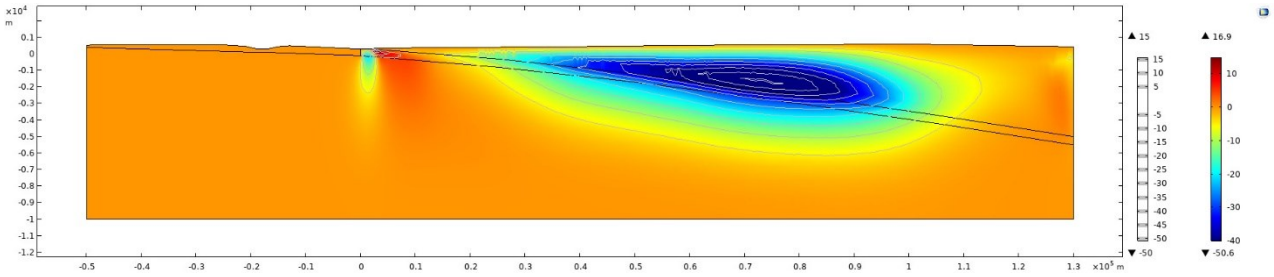

Figure 8: Temperature difference plot (in °C) at 130 ka (representing the present day) with a constant reference surface temperature (i.e. without paleo-temperature forcing) between both scenarios of maximum permeability of 10^{-10} and 10^{-13} m^2 at the Danube, respectively. The vertical exaggeration factor equals 3.

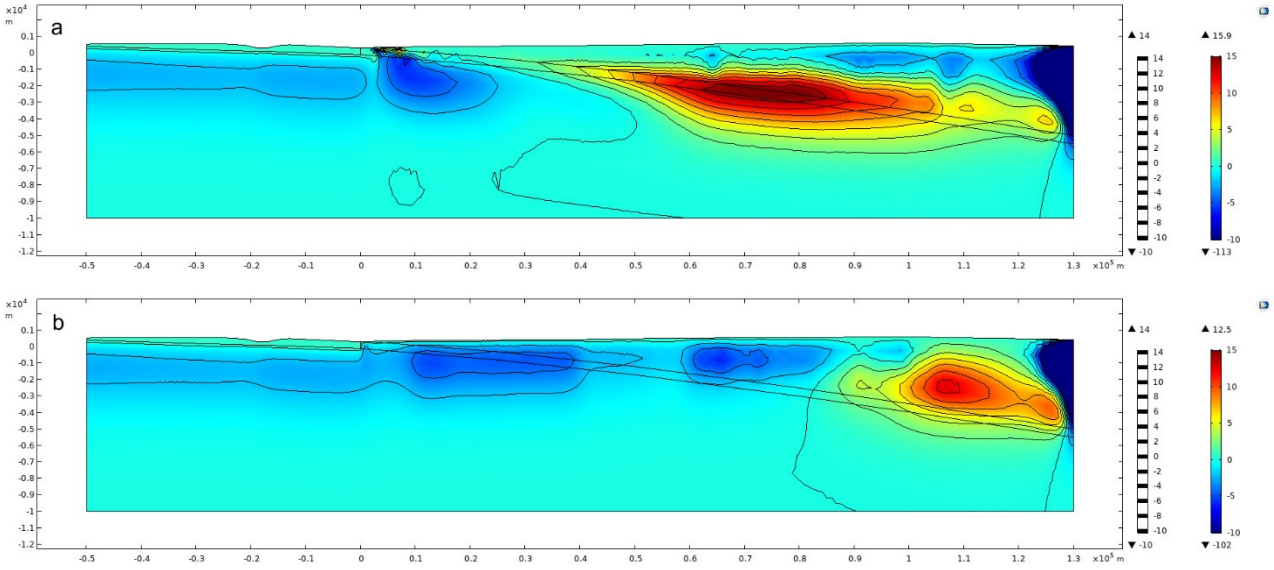

Figure 9: Temperature difference plots (in °C) at 130 ka (representing the present day) between a paleo-temperature forcing and a constant reference temperature of 9°C at 300 m altitude for both the scenarios of maximum permeability of (a) 10^{-10} and (b) 10^{-13} m^2 at the Danube, respectively. The vertical exaggeration factor equals 3.

4. DISCUSSION

Choosing the high carbonate permeability scenario as a reference, three regions with distinct geothermal gradients can be differentiated (Figure 5a). In the Franconian Alb to the north of the Danube valley, the subsurface is cooled by groundwater flowing laterally and downwards to the Altmühl valley. In the region of the Danube valley, the subsurface heats up because this region represents a regional upflow zone. Groundwater from the Franconian Alb but most most importantly from the Molasse Basin circulates deep enough to take up heat and discharge in the Danube valley. Upflow of heated water is known from Bad Gögging which is located 30 km downstream of Ingolstadt (Wirth and Andres 1981). Groundwater and convective heat upflow causes the distance between isotherms to increase because higher temperatures are encountered at shallower depth. According to our model the 20°C-isotherm is located just about 100 m below the surface to the south of the Danube valley (Figure 5 a). By contrast, the Molasse Basin represents a large downflow zone because topography reaches up to 600 m compared to 300 m at the Danube and 440 at the Inn rivers. Here, the distance between isotherms below the main downflow zone decreases, i.e. the isotherms become more densely packed, because the 20°C-isotherm moves to a depth of 2 km (Figure 5a).

The linear variation of Upper Jurassic carbonate permeability along profile A (Figure 5) serves to illustrate the actual situation along profiles located further west (profiles B and C in Figure 1 and Figure 2) where horizontal permeability is as low as 10^{-13} m^2 which is three orders of magnitude lower than in the most karstified carbonate (Birner et al. 2012). The much higher carbonate permeability due to karstification drastically increases the gravity-driven coupled groundwater and heat flow, and thus heat redistribution. The regional redistribution of heat strongly modifies the geothermal gradient. The higher the carbonate permeability, the stronger the gravity-driven groundwater flow which by descending through the Molasse sediments towards the Malm aquifer also significantly cools down the Molasse as well as the carbonate aquifer. By comparing the model with maximum carbonate permeabilities of 10^{-13} and 10^{10} m^2, respectively, the temperature difference or the thermal anomaly created amounts to about -38°C at 130 ka corresponding to the present day (Figure 7). The thermal anomaly is well reflected in the geostatistically evaluated thermal field (Figure 2; Agemar and Tribbensee, 2018). This result therefore confirms that the model is able to replicate the cold thermal anomaly occurring in the

Molasse Basin to the (north-) east of Munich. As a consequence of the thermal anomaly resulting from higher carbonate permeability (Figure 7), maximum permafrost thickness is three to four times thicker (Figure 6). When water freezes, its dynamic viscosity is reduced by about 12 orders of magnitude. Consequently, when permafrost forms, the geological unit becomes practically impermeable. Permafrost formation therefore impedes groundwater flow from the surface.

The calculated temperature difference shown in Figure 8, quite unexpectedly, reveals that the cold thermal anomaly is not principally caused by colder mean annual surface temperatures, permafrost formation or glaciers advancing onto the foreland. Actually, the main cause is the different permeability and thus the magnitude of gravity-driven coupled groundwater and heat flow. Figure 9 visualizes the sole effect of the applied surface temperature boundary condition on both permeability scenarios. The main process of groundwater flow is confirmed in particular by Figure 9a which shows for the high permeability scenario the difference between the models with paleo-temperature forcing and with a constant reference surface temperature only. Despite the on average higher reference temperature (9°C compared to an average of 3.2°C and a median of 2.3°C for paleo-temperature), the thermal anomaly caused by the model with paleo-temperature forcing is paradoxically about 16°C warmer than the model with a constant reference surface temperature. This observation is however explained by reduced groundwater flow caused by periodic permafrost formation. By contrast, even though reference temperature is significantly higher than average or median paleo-temperature, gravity-driven groundwater and heat flow is not disturbed by permeability reduction due to permafrost and thus produces a stronger thermal anomaly of -50°C instead of -38°C (compare Figure 8 and Figure 7d). Another consequence of the model without paleo-climate forcing is 2.6°C warmer water ascending in the Danube valley, which is a reflection of stronger heat redistribution. In Figure 9a, but more so in the more conductive (or less convective) model in Figure 9b, the effect of paleo-temperature is visible beneath the Franconian Alb with a temperature difference of more than -2°C. For both permeability scenarios, the colder zones in the shallow subsurface of the Molasse Basin are remnants of permafrost which retards warming-up. For the low permeability scenario in Figure 9b, the warm anomaly likely is an expression of the two competing processes of (1) primary carbonate permeability and (2) secondary permeability reduction due to permafrost formation. First, the relatively low permeability yields an overall more conductive model, and second, further reduction in permeability and groundwater flow results in less heat redistribution in the deepest part of the Molasse Basin.

5. CONCLUSIONS

This study aimed at using numerical thermal-hydraulic modelling to assess the magnitude of gravity-driven coupled groundwater and heat flow under the paleo-climatic conditions of the last (Würm) glaciation in the south German Molasse Basin as a reference play in order to quantify the potential effect of paleo-climate on basins of the foreland basin play type worldwide. The modelling results confirm that the model is able to replicate the cold thermal anomaly occurring in the Molasse Basin to the (north-) east of Munich. However, the findings are unexpected in regard to the main reason of the observed thermal anomaly. The thermal-hydraulic models show clearly that the cold thermal anomaly is not principally caused by colder mean annual surface temperatures, permafrost formation, or glaciers advancing onto the foreland. In the high carbonate permeability, more convective, scenario, permafrost formation produces not a thermal but a hydraulic blanketing or shielding effect and reduces heat redistribution so as to create a positive thermal anomaly centered on the Molasse Basin and the Malm carbonate aquifer. Models performed with the higher reference surface temperature yields a significantly colder thermal anomaly because groundwater flow reduction due to permafrost is absent. To sum up, the strength of the thermal anomaly is essentially related to the magnitude of gravity-driven coupled groundwater and heat flow.

REFERENCES

Agemar, T., and Tribbensee, K.: GeotIS-Verbundmodell des Top-Malm im Bereich des nördlichen Vorlandbeckens der Alpen, *Zeitschrift der Deutschen Gesellschaft für Geowissenschaften*, **169**, (2018), 335-341.

Andres, G., and Frisch, H.: Hydrogeologie und Hydraulik im Malmkarst des Molassebeckens und der angrenzenden Fränkisch-Schwäbischen Alb, in: Schriftenreihe Bayer. Landesamt für Wasserwirtschaft, vol 15. Bayer. Landesamt für Wasserwirtschaft, München, (1981), pp 108-117.

Bachmann, G.H., Dohr, G., and Mueller, M.: Exploration in a classic thrust belt and its foreland; Bavarian Alps, Germany, *AAPG Bulletin*, **66**, (1982), 2529-2542.

Bachmann, G.H., and Mueller, M.: Sedimentary and structural evolution of the German Molasse Basin, *Eclogae Geologicae Helvetiae*, **85**, (1992), 519-530.

Bachmann, G.H., Mueller, M., and Weggen, K.: Evolution of the Molasse Basin (Germany, Switzerland), *Tectonophysics*, **137**, (1987), 77-92.

Birner, J.: Hydrogeologisches Modell des Malmaquifers im Süddeutschen Molassebecken. *PhD Thesis*, Freie Universität Berlin, Germany, (2013).

Birner, J., Fritzer, T., Jodocy, M., Savvatis. A., Schneider, M., and Stober, I.: Hydraulische Eigenschaften des Malmaquifers im Sueddeutschen Molassebecken und ihre Bedeutung fuer die geothermische Erschliessung, *Zeitschrift für Geologische Wissenschaften*, **40**, (2012), 133-156.

Böhm, F.: Die Lithofazies des Oberjura (Malm) im Großraum München und deren Einfluss auf die geothermische Nutzung, *PhD Thesis*, Freie Universität Berlin, Germany, (2012).

Brink, H.-J., Burri, P., Lunde, A., and Winhard, H.: Hydrocarbon habitat and potential of Swiss and German Molasse Basin; a comparison, *Eclogae Geologicae Helvetiae*, **85**, (1992), 715-732.

Freudenberger, W., and Schwerd, K.: Erläuterungen zur Geologischen Karte von Bayern 1:500000. 4., neubearb. Aufl. edn. Bayer. Geolog. Landesamt, München, Germany, (1996).

Frisch, H., and Huber, B.: Ein hydrologisches Modell und der Versuch einer Bilanzierung des Thermalwasservorkommens für den Malmkarst im Süddeutschen und im angrenzenden Oberösterreichischen Molassebecken, *Proceedings*, IV. Würzburger Hydrogeologisches Kolloquium 1998, Institut für Geologie der Universität München, Germany, (2000), pp 25-43.

GeoMol Team: GeoMol - assessing subsurface potentials of the Alpine Foreland Basins for sustainable planning and use of natural resources, *Project report*, Bavarian Environment Agency, Augsburg, Germany, (2015).

Goldscheider, N., Madl-Szonyi, J., Eross, A., and Schill, E.: Review; thermal water resources in carbonate rock aquifers, *Hydrogeology Journal*, **18**, (2010), 1303-1318.

Hänel, R., and Staroste, E.: Atlas of geothermal resources in the European Community, Austria and Switzerland, *Report*, EUR 11026. Commission of the European Communities, Brussels-Luxembourg, (1988).

Jodocy, M., and Stober, I.: Geologisch-geothermische Tiefenprofile fuer den suedwestlichen Teil des Sueddeutschen Molassebeckens, *Zeitschrift der Deutschen Gesellschaft fuer Geowissenschaften*, **160**, (2009), 359-366.

Jouzel, J., et al.: Orbital and millennial Antarctic climate variability over the past 800,000 years, *Science*, **317**, (2007), 793-796.

Kuhlemann, J., and Kempf, O.: Post-Eocene evolution of the North Alpine foreland basin and its response to Alpine tectonics, *Sedimentary Geology*, **152**, (2002), 45-78.

Lemcke, K., and Tunn, W.: Tiefenwasser in der sueddeutschen Molasse und in ihrer verkarsteten Malmunterlage, *Bulletin der Vereinigung Schweizerischer Petroleum -Geologen und –Ingenieure*, **23**, (1956), 35-56.

Meyer, R.K.F., and Schmidt-Kaler, H.: Palaeogeographie und Schwammriffentwicklung des sueddeutschen Malm; ein Ueberblick, *Facies*, **23**, (1990), 175-184.

Moeck, I.S.: Catalog of geothermal play types based on geologic controls, *Renewable and Sustainable Energy Reviews*, **37**, (2014), 867-882.

Moeck, I.S., and Beardsmore, G.: A new 'geothermal play type' catalog: Streamlining exploration decision making, *Proceedings*, 29th Workshop on Geothermal Reservoir Engineering, Stanford University, Stanford, CA, (2014).

Moeck, I.S., Beardsmore, G., and Harvey, C.C.: Cataloging worldwide developed geothermal systems by geothermal play type, *Proceedings*, World Geothermal Congress, Melbourne, Australia, (2015).

Przybycin, A.M., Scheck-Wenderoth, M., Schneider, M.: The origin of deep geothermal anomalies in the German Molasse Basin: results from 3D numerical models of coupled fluid flow and heat transport, *Geothermal Energy*, **5:1**, (2017).

Reinecker, J., Tingay, M., Mueller, B., and Heidbach, O.: Present-day stress orientation in the Molasse Basin, *Tectonophysics*, **482**, (2010), 129-138.

Reischenbacher, D., and Sachsenhofer, R.F.: Entstehung von Erdgas in der oberoesterreichischen Molassezone; Daten und offene Fragen, *BHM Berg Huettenmaenn Monatsh.*, **156**, (2011), 463-468.

Roeder, D., and Bachmann, G.: Evolution, structure and petroleum geology of the German Molasse Basin, *Memoires du Museum National d'Histoire Naturelle (Paris, France)*, **170**, (1996), 263-284.

Rühaak, W.: Multidimensional modeling of the thermal and flow regime in the western part of the Molasse Basin, Southern Germany, *PhD Thesis*, Rheinisch-Westfälische Technische Hochschule, Aachen, Germany, (2009).

Sachsenhofer, R.F., Gratzer, R., Tschelaut, W., and Bechtel, A.: Characterisation of non-producible oil in Eocene reservoir sandstones (Bad Hall Nord Field, Alpine Foreland Basin, Austria), *Marine and Petroleum Geology*, **23**, (2006), 1-15.

Schintgen, T., Foerster, A., Foerster, H.-J., and Norden, B.: Surface heat flow and lithosphere thermal structure of the Rhenohercynian zone in the greater Luxembourg region, *Geothermics*, **56**, (2015), 93-109.

Schmid, S.M., Fuegenschuh, B., Kissling, E., and Schuster, R.: Tectonic map and overall architecture of the Alpine orogeny, *Eclogae Geologicae Helvetiae*, **97**, (2004), 93-117.

Seguinot, J., Ivy-Ochs, S., Jouvet, G., Huss, M., Funk, M., and Preusser, F.: Modelling last glacial cycle ice dynamics in the Alps, *The Cryosphere (Online)*, **12**, (2018), 3265-3285.

Seipold, U.: Der Wärmetransport in kristallinen Gesteinen unter den Bedingungen der kontinentalen Kruste, *Report*, GeoForschungsZentrum Potsdam, Potsdam, Germany, (2001).

Somerton, W.H.: Thermal properties and temperature-related behavior of rock/fluid systems, *Developments in Petroleum Science*, *37*, (1992).

Stober, I., Wolfgramm, M., and Birner, J.: Hydrochemie der Tiefenwässer in Deutschland, *Zeitschrift für geologische Wissenschaften*, **41/42**, (2014), 339-380.

Toth, J.: Gravitational systems of groundwater flow; theory, evaluation, utilization, Cambridge University Press, New York, NY, (2009).

Wagner, W., and Kretzschmar, H.-J.: International Steam Tables. Properties of Water and Steam based on the Industrial Formulation IAPWS-IF97, 2nd ed., Springer, Berlin, Heidelberg, Germany, (2008).

Wirth, H., and Andres, G.: Die Thermal- und Schwefelwasservorkommen von Bad Goegging; Mit Beitraegen zum geologisch-tektonischen Rahmen sowie zur Hydraulik des Tiefenwassers im Malmkarst des Molassebeckens, *Schriftenreihe des Bayerischen Landesamtes fuer Wasserwirtschaft*, **15**, Munich, Germany, (1981).